Permanent neuroglial remodeling of the retina following infiltration of CSF1R inhibition-resistant peripheral monocytes

Eleftherios I. Paschalis[a,b,c,1,2], Fengyang Lei[a,b,c,2], Chengxin Zhou[a,b,c], Vassiliki Kapoulea[a,b,c], Reza Dana[a], James Chodosh[a,b,c], Demetrios G. Vavvas (Δημήτριος Γ. Βάββας)[a,d,3], and Claes H. Dohlman[a,b,3]

[a]Department of Ophthalmology, Massachusetts Eye and Ear Infirmary, Harvard Medical School, Boston, MA 02114; [b]Boston Keratoprosthesis Laboratory, Schepens Eye Research Institute, Massachusetts Eye and Ear Infirmary, Harvard Medical School, Boston, MA 02114; [c]Disruptive Technology Laboratory, Department of Ophthalmology, Massachusetts Eye and Ear Infirmary, Harvard Medical School, Boston, MA 02114; and [d]Angiogenesis Laboratory, Department of Ophthalmology, Massachusetts Eye and Ear Infirmary, Harvard Medical School, Boston, MA 02114

Edited by Kenneth M. Murphy, Washington University School of Medicine, St. Louis, MO, and approved October 24, 2018 (received for review May 14, 2018)

Previous studies have demonstrated that ocular injury can lead to prompt infiltration of bone-marrow–derived peripheral monocytes into the retina. However, the ability of these cells to integrate into the tissue and become microglia has not been investigated. Here we show that such peripheral monocytes that infiltrate into the retina after ocular injury engraft permanently, migrate to the three distinct microglia strata, and adopt a microglia-like morphology. In the absence of ocular injury, peripheral monocytes that repopulate the retina after depletion with colony-stimulating factor 1 receptor (CSF1R) inhibitor remain sensitive to CSF1R inhibition and can be redepleted. Strikingly, consequent to ocular injury, the engrafted peripheral monocytes are resistant to depletion by CSF1R inhibitor and likely express low CSF1R. Moreover, these engrafted monocytes remain proinflammatory, expressing high levels of MHC-II, IL-1β, and TNF-α over the long term. The observed permanent neuroglia remodeling after injury constitutes a major immunological change that may contribute to progressive retinal degeneration. These findings may also be relevant to other degenerative conditions of the retina and the central nervous system.

glaucoma | PLX5622 | neurodegeneration | macrophage | neuroprotection

We recently showed that acute ocular surface injury causes prompt infiltration of peripheral monocytes into the retina (1). These cells gradually differentiate from ameboid C-C chemokine receptor 2^+ ($CCR2^+$) monocytes to highly ramified CX3C chemokine receptor 1^+ ($CX3CR1^+$)-expressing macrophages (1) and acquire a morphology that resembles microglia. However, how these cells functionally integrate into the retina has not been investigated. Understanding the contribution of peripheral monocytes in retinal neuroglia remodeling may be clinically important to our understanding of mechanisms involved in progressive neuroretinal degeneration, especially after ocular injuries, since depletion/antagonism strategies may be employed therapeutically for patients with neuroglia disorders (2, 3).

Peripheral monocytes/macrophages share a common lineage with microglia, complicating the study of the subsequent differentiation of these two cell populations (4). Recently, new markers have been proposed for labeling microglia (5, 6); however, they still require further validation. Traditionally, studies have involved the use of transgenic mice and bone-marrow chimeras, but such studies have often generated confusion, primarily due to side effects from gamma irradiation used in bone-marrow transfer (BMT) which can result in blood–brain barrier disruption (4, 7–9) and peripheral monocyte infiltration. Thus, the presence of peripheral monocytes after BMT was initially attributed to a physiological microglia turnover by peripheral monocytes. However, improved fate-mapping techniques have now confirmed that peripheral monocytes/macrophages do not enter into the CNS or retina parenchyma under normal conditions (1, 10, 11). Therefore, such infiltration happens only in pathologic conditions (8) and likely contributes to neuroinflammation (1, 12, 13).

This study was designed to examine the ontogeny and function of peripheral infiltrating macrophages into the retina after ocular injury (14). To address these questions, we employed our previously characterized busulfan myelodepletion bone-marrow chimera model for long-term fate mapping of peripheral monocyte infiltration into the retina (1). In addition, we used a small-molecule inhibitor of colony-stimulating factor 1 receptor (CSF1R) to perform a set of microglia-depletion experiments to study the roles of microglia and peripheral monocytes in retinal repopulation. This study shows that peripheral monocytes not only are responsible for acute retinal inflammation after ocular injury (1, 14) but also contribute to the permanent remodeling of the neuroglia system by establishing a proinflammatory phenotype that may promote or contribute to neurodegeneration. These findings may be clinically important and can help us better understand the mechanisms by which patients with acute chemical, surgical, or

Significance

This work contributes to the understanding of the enigmatic progressive retinal damage following acute ocular surface injury. Clinical findings in patients suggest that such injuries can adversely affect the retina. This study demonstrates that corneal injury leads to rapid infiltration of blood-derived monocytes into the retina and to subsequent remodeling of the neuroglial system. In contrast to previously held belief, this study shows that the blood-derived monocytes engraft permanently into the retina and differentiate into microglia-like cells. Although these cells are morphologically indistinguishable from native microglia, they retain a distinct signature and insensitivity to CSF1R inhibition and exhibit a reactive phenotype which persists long after the noxious stimuli is removed, ultimately contributing to progressive neuroretinal degeneration.

Author contributions: E.I.P. and D.G.V. designed research; E.I.P. and F.L. performed research; E.I.P. and J.C. contributed new reagents/analytic tools; E.I.P., F.L., C.Z., and V.K. analyzed data; E.I.P., R.D., J.C., D.G.V., and C.H.D. wrote the paper; and R.D., J.C., D.G.V., and C.H.D. provided guidance and edited versions of the paper.

The authors declare no conflict of interest.

This article is a PNAS Direct Submission.

[1]To whom correspondence should be addressed. Email: Eleftherios_Paschalis@MEEI.HARVARD.EDU.

[2]E.I.P. and F.L. contributed equally to this work.

[3]D.G.V. and C.H.D. contributed equally to this work.

This article contains supporting information online at www.pnas.org/lookup/suppl/doi:10.1073/pnas.1807123115/-/DCSupplemental.

Published online November 15, 2018.

traumatic ocular injuries become susceptible to progressive neurodegeneration processes such as progressive retinal ganglion cell loss (glaucoma) (1, 15) long after the injury has taken place.

Results

Ocular Injury Leads to Infiltration and Permanent Engraftment of Blood-Derived Monocytes into the Retina. We recently showed that corneal alkali injury results in peripheral monocyte infiltration to the retina within 24 h (1). These cells adopt a dendritiform morphology within 7 d and appear to integrate into the retina (1). To determine the long-term effect of the peripheral monocyte infiltration into the retina, we employed a $CX3CR1^{+/EGFP}$::$CCR2^{+/RFP}$ bone-marrow chimera model which maps the fate $CCR2^{+}$ monocyte-derived $CX3CR1^{+}$ cells. Myelodepletion was performed with busulfan instead of gamma irradiation, since busulfan treatment was recently shown not to cause peripheral monocyte infiltration into the retina of bone-marrow–transferred mice (1). To minimize confounding, the contralateral eye of each mouse was used as an internal control.

In the absence of retinal injury peripheral $CX3CR1^{+}$ cells do not physiologically infiltrate into the retina 16 mo after BMT (Fig. 1). Only a small number of $CX3CR1^{+}$ cells is present around the optic nerve head (red arrows in Fig. 1 *A* and *F*) and along the retinal vessels (white arrows in Fig. 1) (Fig. 1 *A*, *D*, *F*, and *I*). However, peripheral $CCR2^{+}$ monocytes are present in the inner retina (Fig. 1 *B*, *E*, *G*, and *J*), appearing as "patrolling" retinal monocytes, corroborating our earlier findings (1). Very few of these peripheral $CX3CR1^{+}$ cells coexpress CCR2 (Fig. 1 *C* and *H*). In contrast, after ocular injury, the retina is populated almost entirely (~93%) by peripheral $CX3CR1^{+}$ cells (Fig. 1*D*) that appear to engraft into the tissue permanently (16 mo postinjury) (Fig. 1 *D*, *I*, *K*, and *L*). Peripheral $CX3CR1^{+}$ cells appear highly dendritic, morphologically resembling yolk-sac microglia. These cells migrated and occupied all three distinct retinal microglia strata [the ganglion cell layer (GCL), the inner plexiform layer (IPL)/inner nuclear layer (INL), and the outer plexiform layer (OPL)] in an orderly fashion, as yolk-sac microglial cells do (Fig. 1 *M–O* and Movie S1). The extent of peripheral $CX3CR1^{+}$ monocyte presence in the retina 16 mo after the injury appears to cause permanent retinal neuroglia remodeling that does not involve an increase in $CCR2^{+}$ cell number (Fig. 1 *E*, *J*, *P*, and *Q*). Peripheral $CCR2^{+}$ cells also occupy the three distinct retinal microglia strata (GCL, IPL/INL, and OPL) (Fig. 1 *R–T*) but without coexpressing the CX3CR1 marker (Fig. 1 *U* and *V*). These cells represent a population of peripheral progenitor monocytes that can mature to $CCR2^{-}$ $CX3CR1^{+}$ cells and give rise to tissue-resident macrophages after ocular injury (1). Sixteen months after the removal of the noxious stimulus, these cells appeared to resume their apparent patrolling function as peripheral progenitor $CCR2^{+}$ cells. A representative schematic of the flat-mount retina is provided in Fig. 1*W*.

Infiltrated Peripheral $CX3CR1^{+}$ Cells Remain Proinflammatory Months After Engraftment Despite Their Ramified Quiescent Morphology. We previously showed that peripheral monocyte infiltration into the retina is associated with marked neuroretinal tissue damage (1). Prompt inhibition of the monocyte infiltration using the TNF-α inhibitor infliximab leads to retinal protection (1). To assess the nature of peripheral $CX3CR1^{+}$ monocytes engrafted into the retina, we employed a BMT model and flow cytometry to assess the expression of MHC-II, IL-1β, and TNF-α, which serve as indicators of cell activation. Five months after ocular injury, 72% of the $CX3CR1^{+}$ $CD45^{hi}$ cells are $MHC\text{-}II^{hi}$ despite their otherwise quiescent morphology (Fig. 2 *A* and *B*). At the same time, 79% of the $CX3CR1^{+}$ $CD45^{lo}$ cells are $MHC\text{-}II^{-}$ (Fig. 2 *A* and *B*). Using dual color labeling in $CX3CR1^{+/EGFP}$ chimeras, we managed to differentiate peripheral $CX3CR1^{+}$ ($EGFP^{+}/RFP^{+}$) cells from $EGFP^{-}/RFP^{+}$ embryonic microglia and study their inflammatory expression (Fig. 2*C*). Although both populations of cells expressed IL-1β and TNF-α 16 wk after injury, peripheral $CX3CR1^{+}$ cells exhibited statistically significantly stronger expression than yolk-sac–derived microglia (Fig. 2*E*). Peripherally engrafted $CX3CR1^{+}$ cells were also shown to engulf $\beta3\text{-tubulin}^{+}$ tissue 20 wk after the injury despite their apparent quiescent morphology (Fig. 2 *F* and *G*), suggesting prolonged and active phagocytosis of the neuroretinal tissue (Fig. 2 *F* and *G* and Movie S2). In contrast, embryonic microglia did not interact with $\beta3\text{-tubulin}^{+}$ tissue in steady-state conditions (Fig. 2 *H* and *I* and Movie S2).

Ocular Injury Causes Peripherally Engrafted Microglia to Become Resistant to CSFR1 Inhibition. To further characterize the nature of the retina-engrafted monocytes after ocular injury, we performed microglia ablation using systemic administration of PLX5622, a small molecule that inhibits CSF1R and leads to microglia depletion (16, 17). First, we assessed the ability of PLX5622 to deplete retinal microglia. Administration of PLX5622 for 3 wk completely removed retinal microglia from $CX3CR1^{+/EGFP}$ mice not subjected to ocular injury. This event was followed by a gradual repopulation of the retina within 3 wk. The repopulating cells migrated into the three distinct retinal microglia strata (GCL, IPL/INL, and OPL) and transformed to a dendritiform morphology. PLX5622 treatment was performed in bone-marrow–transferred mice to assess the contribution of peripheral monocytes in microglia repopulation (Fig. 3*A*). These repopulating cells were primarily from the periphery (Fig. 3 *B–M*) with a small number (~7%) originating from nonperipheral microglia progenitors, whose contribution increased after acute ocular injury (~20%) (*SI Appendix*, Fig. S1). Repopulating cells migrate into the three distinct microglia strata within 6 wk of cessation of PLX5622 treatment (Fig. 3 *N–P*). These repopulated cells remained sensitive to the CSF1R inhibitor and could be reablated by readministration of PLX5622 (Fig. 3 *Q–U*). In contrast, in the setting of ocular injury, peripherally engrafted monocytes were resistant to the CSF1R inhibitor and could not be ablated with PLX5622 treatment (Fig. 4 *A–H*). These cells appeared semiramified, occupying all three distinct microglia strata (Fig. 4 *I–K*) but with higher density in the OPL (Fig. 4*K*), likely due to local migration. The resistance of retinal microglia that populated the retina after ocular injury to PLX5622 treatment was not due to their peripheral origin, since repopulated microglia in the absence of ocular injury also originated from the periphery (Fig. 3 *F* and *L*) and remained sensitive to PLX5622 after engraftment (Fig. 3 *R*, *S*, and *U*). Resistance of $CX3CR1^{+}$ cells to the CSF1R inhibitor is likely due to reduced expression of CSF1R by these cells (*SI Appendix*, Fig. S2).

Further ex vivo functional analysis was performed in retinal $CSF1R^{+}$ and $CSF1R^{-}$ $CX3CR1^{+}$ cells from $CX3CR1^{+/EGFP}$ mice that were isolated using flow cytometry 3 wk after ocular injury or from naive mice (Fig. 4 *L*, *M*, *O*, and *P*). Cells were cultured for 5 d with or without recombinant CSF1 and IL-4 stimulation (16, 18–20). BrdU was used to assess cell proliferation. $CSF1R^{-}$ cells from both naive and injured eyes were not influenced or rescued by CSF1 and IL-4 stimulation and did not survive the 5-d culture (Fig. 4*N*). In contrast, $CSF1R^{+}$ cells were rescued with CSF1 and IL-4 stimulation and showed increased proliferation and BrdU retention (Fig. 4*N*).

Discussion

Here, we show that ocular injury not only causes peripheral monocyte infiltration into the retina, as previously demonstrated (1), but also leads to permanent engraftment and remodeling of the neuroglia system to a proinflammatory state resistant to CSFR1 inhibition. This process is characterized by (*i*) infiltration of peripheral $CX3CR1^{+}CCR2^{+}$ cells into the retina within hours after the injury; (*ii*) migration of these cells into the three distinct microglia strata (GCL, IPL/INL, and OPL); (*iii*) differentiation of these cells

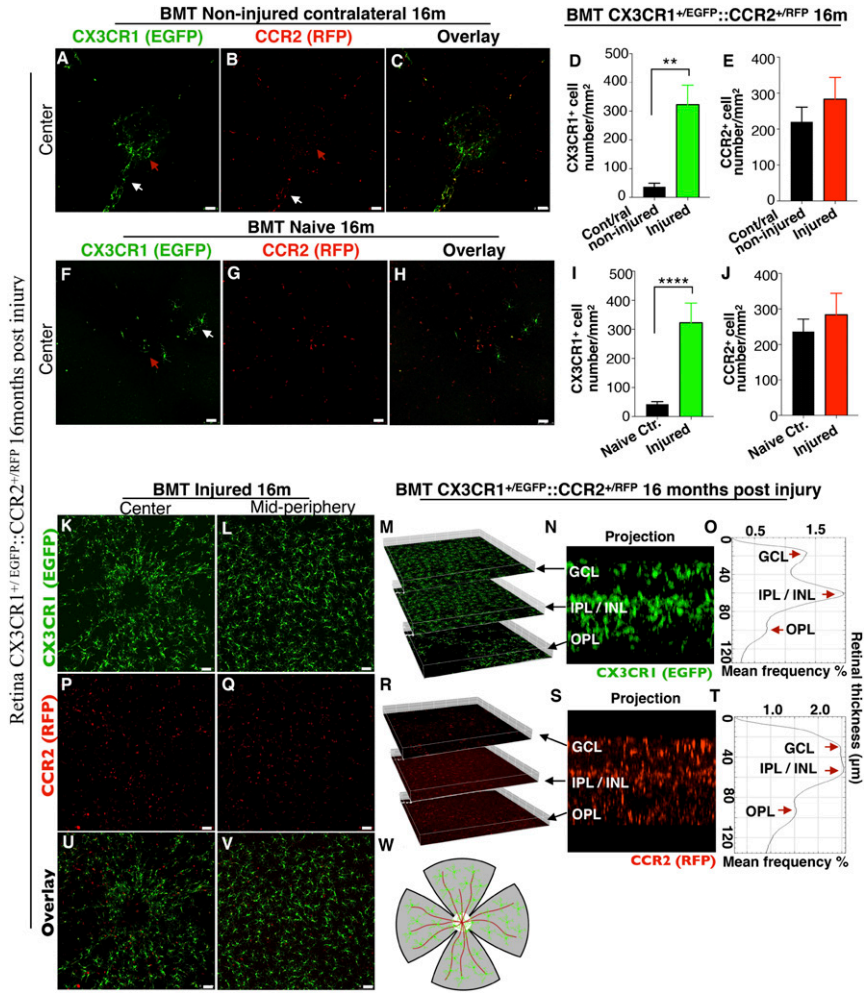

Fig. 1. Ocular injury causes permanent engraftment in the retina of peripheral CX3CR1$^+$ cells which adopt microglia morphology. (*A–C* and *F–H*) Confocal microscopy of busulfan-myelodepleted and bone-marrow–transferred mice with CX3CR1$^{+/EGFP}$::CCR2$^{+/RFP}$ cells 16 mo after corneal alkali burn injury. Maximum projection of confocal images shows that CX3CR1$^+$ cells cannot enter into the retina of the contralateral noninjured eye 16 mo after injury (*A*), nor can they populate the retina of naive eyes under physiological conditions (*F*). Few cells are present around the optic nerve head (red arrow) and along the major retinal vessels (white arrow). Maximum projection of confocal images shows CCR2$^+$ cells are scattered across the retina of the contralateral noninjured (*B*) and of the naive (*G*) eye, located mainly in the GCL. *C* and *H* show overlay images of CX3CR1 and CCR2 channels. (*D*, *E*, *I*, and *J*) Quantification of the number of peripheral CX3CR1$^+$ and CCR2$^+$ cells 16 mo after ocular injury shows a marked increase in CX3CR1$^+$ cells ($P < 0.003$) but normal numbers of CCR2$^+$ cells ($P > 0.415$) compared with contralateral noninjured and naive eyes. Data in *D* and *E* are presented as mean ± SD, paired *t* test. Data in *I* and *J* are presented as mean ± SD, independent *t* test. $^{**}P < 0.01$; $^{****}P < 0.0001$. (*K* and *L*) Ocular injury causes infiltration and permanent engraftment of peripheral CX3CR1$^+$ cells in the retina. (*M–O*) Sixteen months after the injury, infiltrated CX3CR1$^+$ cells migrate into the three distinct microglia strata (GCL, IPL/INL, OPL) and adopt dendritiform microglia morphology. (*M*) Isometric reconstruction of confocal stacks separated by retinal layers (GCL, IPL/INL, and OPL). (*N*) A cross-section of the retina shows the presence of CX3CR1$^+$ cells in the GCL, IPL/INL, and OPL. (*O*) A histogram of CX3CR1$^{+/EGFP}$ expression within the retinal tissue shows intensity peaks of EGFP signal in the GCL, IPL/INL, and OPL. (*P* and *Q*) Patrolling CCR2$^+$ cells are present in the retina but do not differentiate into CX3CR1$^+$ cells. (*R–T*) Even though the number of peripheral CCR2$^+$ cells is normal, peripheral CCR2$^+$ cells are present in all three distinct microglia strata (GCL, IPL/INL, and OPL) 16 mo after the injury. In *O* and *T* the thickness of the retinal tissue and the relative position of each microglia stratum was derived automatically by the confocal system (Leica SP8) and was calculated by multiplying the number of serial confocal scans by the step of each scan in micrometers. (*U* and *V*) Overlay images of CX3CR1 and CCR2 channels 16 mo after ocular injury. (*W*) A representative schematic of a flat-mount retina as used for confocal imaging. The center white circle represents the optic nerve head, red lines represent the retinal vessels, and green dots represent the peripheral monocytes. (Scale bars: 50 µm in *A–C*, *F–H*, *K*, *L*, *P*, *Q*, *U*, and *V*.) $n \geq 5$ mice per group.

to dendritiform cells; and, finally, (*iv*) permeant engraftment of these cells into the retina as tissue-resident CX3CR1$^+$CCR2$^-$ monocytes. Interestingly, despite their integration into the tissue and their morphometric resemblance to yolk-sac–derived microglia, these cells remain different from yolk-sac–derived microglia. Unlike native microglia, peripherally engrafted monocytes retain expression of the activation marker MHC-II, are actively involved in phagocytosis of the neuroretinal tissue, and become resistant to the CSF1R inhibitor despite their otherwise quiescent morphology and integration into the retina.

Using PLX5622, a small-molecule inhibitor of CSF1R (an essential receptor for microglia survival), we show that peripheral CX3CR1$^+$ monocytes engrafted after injury differ from the yolk-sac–derived microglia and cannot be ablated using CSF1R inhibition. In contrast, peripheral CX3CR1$^+$ cells repopulating in the absence of ocular injury remain sensitive to PLX5622 treatment and can be reablated. On one hand, the findings could be due to the progeny of the infiltrating cell type and perhaps the existence of bone-marrow cells that give rise to postembryonic self-maintaining tissue-resident macrophages. On the other hand, they could be due to

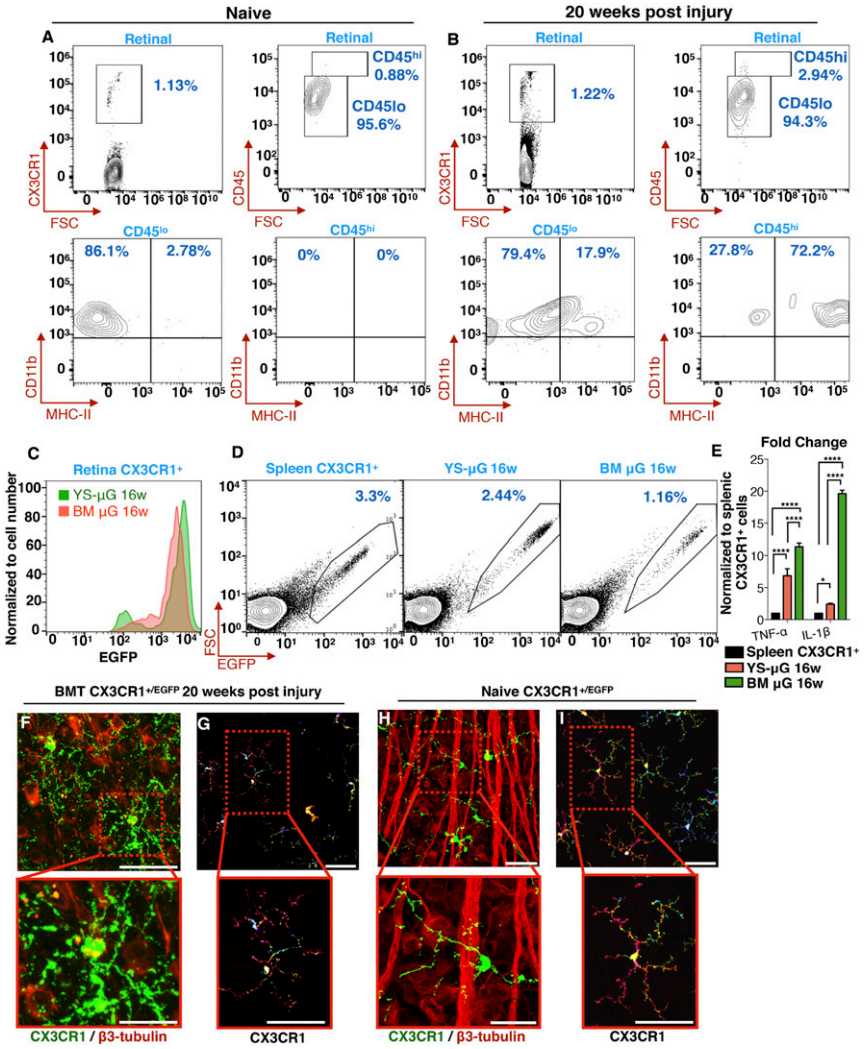

Fig. 2. Engrafted peripheral CX3CR1^{+} cells remain reactive despite their morphometric quiescence. (*A–D*) Flow cytometric analysis of retinal cells from CX3CR1$^{+/EGFP}$ mice. (*A*) In naive mice, CX3CR1^{+} cells are predominantly CD45^{lo} (96%), and only a small percentage is CD45^{hi} (4%). CX3CR1^{+} CD45^{lo} cells do not express MHC-II; however, 2.8% of CX3CR1^{+} CD45^{hi} cells have baseline MHC-II expression. (*B*) Twenty weeks after ocular injury, 94% percent of the CX3CR1^{+} cells are CD45^{lo}, 20% of which express MHC-II. Likewise, 3% of the CX3CR1^{+} cells are CD45^{hi}, 72% of which express MHC-II. (*C*) Flow cytometry for the differentiation of yolk-sac–derived retinal microglia (YS-µGlia 16w) from peripherally engrafted bone-marrow CX3CR1^{+} monocytes (MB µG 16w) 16 wk after ocular injury using RFP-conjugated CX3CR1 antibody against bone-marrow–transferred CX3CR1$^{+/EGFP}$ retinal cells. Both cell populations are strongly expressed. (*D*) Flow cytometry and cell sorting of splenic CX3CR1^{+} cells (control), retinal yolk-sac–derived microglia, and retinal peripherally engrafted monocytes 16 wk after ocular injury for subsequent analysis of IL-1β and TNF-α expression with qPCR. (*E*) Compared with splenic CX3CR1^{+} cells, both yolk-sac–derived and peripheral microglia had elevated TNF-α and *IL-1β* gene expression. However, peripherally engrafted monocytes had significantly higher expression than yolk-sac–derived microglia 16 wk after injury. *$P < 0.05$; ****$P < 0.0001$; Tukey's method for multiple comparisons. (*F* and *G*) Twenty weeks after the injury, peripheral CX3CR1^{+} monocytes appear to frequently interact with and engulf β3 tubulin^{+} neuroretinal tissue (*F*), despite their otherwise ramified and quiescent morphology (*G*). (*H* and *I*) In contrast, in naive eyes, although ramified CX3CR1^{+} monocytes come into contact with β3 tubulin^{+} neuronal tissue, they do not internalize it. (Scale bars: *F–I*, *Upper*, 50 µm; *F–I*, *Lower*, 20 µm.) All experiments were performed in triplicate.

epigenetic effects stemming from the injury leading to changes in gene expression and subsequent changes in the phenotype. Indeed, epigenetic reprogramming can occur in brain microglia after exposure to inflammatory mediators such as TNF-α, IL-1β, and IL-6 (21). This effect persists for months and leads to microglia immune training and tolerance. Therefore, altering microglia epigenetic reprogramming through cytokine manipulation may be a potential therapeutic avenue for retina and brain neuropathology (21, 22).

Previous studies have shown that at 7 d after injury infiltrated peripheral monocytes in the CNS remain transcriptionally similar to peripheral myeloid cells (23) and distinctly different from microglia (5, 24–28). The lack of adaptation of recruited peripheral monocytes in the CNS environment may contribute to functional neuroglia changes and subsequent damage to the tissue (23). Whether CSF1R resistance is due to epigenetic reprogramming or to selective recruitment of distinct progenitor cells that do not express CSF1R is not known and merits further investigation. However, recent reports have demonstrated the existence of two waves of temporally separated and functionally distinct monocyte progenitors that emerge from the yolk sac between E7.5 and E.8.5 (29). The first wave consists of CSF1R^{hi} c-Myb^{-} monocyte progenitors giving rise to mostly local macrophages and microglia without monocyte intermediates. The second wave consists of CSF1R^{lo} c-Myb^{+} monocyte progenitors which give rise locally to yolk-sac macrophages. Most of these latter cells migrate into the fetal liver through the blood circulation at E9.5 to generate cells of multiple lineages (29). They likely represent cells that transiently become progenitors and precursors for the majority of

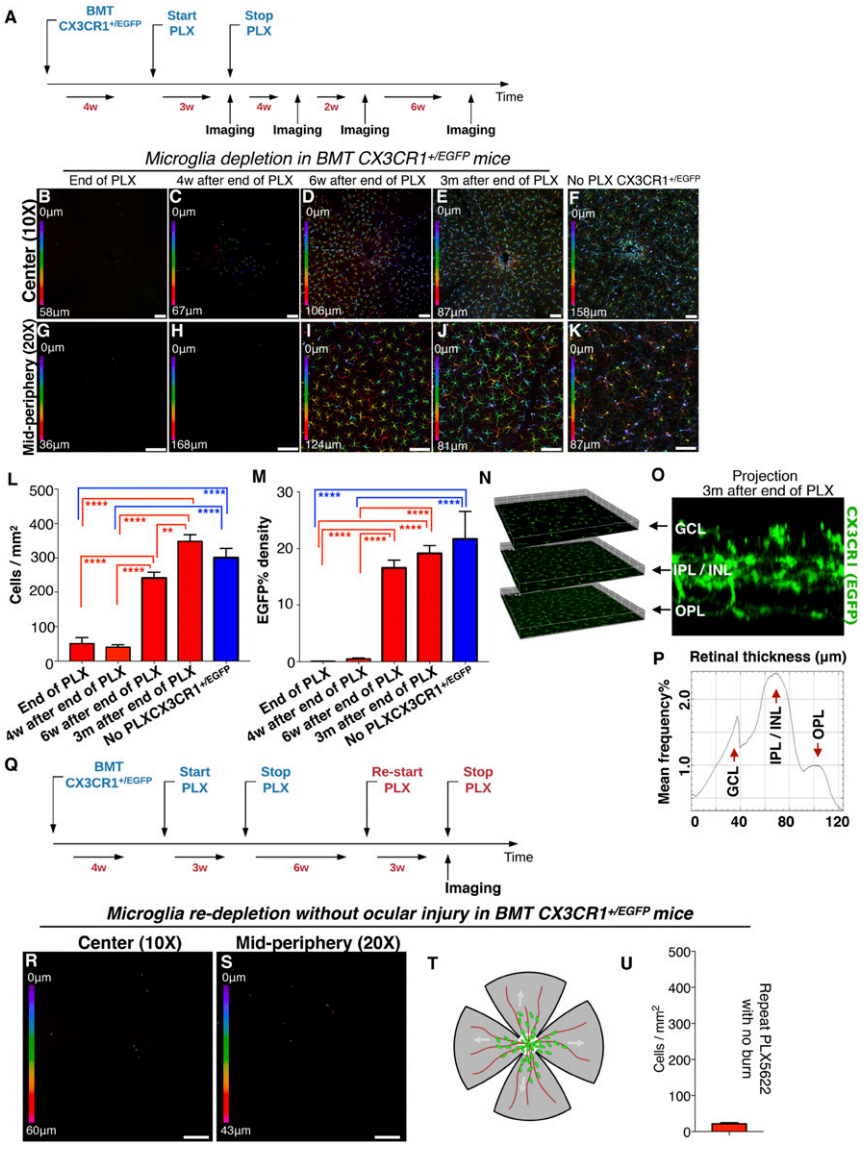

Fig. 3. Microglia repopulation after PLX5622 treatment occurs primarily by peripheral CX3CR1^{+} cells. (*A*) Schematic of the experiment: Busulfan-myelodepleted C57BL/6 mice received adoptive transfer of CX3CR1$^{+/EGFP}$ bone-marrow cells. Four weeks later they received PLX5622 treatment for 3 wk followed by confocal microscopy 3 wk after the cessation of PLX5622 treatment. (*B–F*) Central color-depth–coded (0 represents innermost retina) confocal images of flat-mount retinas 0, 4, 6 wk, and 3 mo after cessation of PLX5622 treatment (*B–E*) and of naive CX3CR1$^{+/EGFP}$ mice (*F*). (*G–K*) Midperipheral color-depth–coded confocal images of flat-mount retinas 0, 4, 6 wk, and 3 mo after cessation of PLX5622 treatment (*G–J*) and of naive CX3CR1$^{+/EGFP}$ mice (*K*). (Scale bars: 100 μm.) (*L*) Quantification of CX3CR1^{+} cell number at the indicated times post PLX5622 treatment. (*M*) Quantification of EGFP intensity at the indicated times post PLX5622 treatment. $^{**}P < 0.01$, $^{****}P < 0.0001$; Tukey's multiple-comparisons method. PLX5622 treatment for 3 wk does not cause acute peripheral CX3CR1^{+} cell infiltration into the retina (*B*, *F*, *G*, *L*, and *M*). However, 6 wk after cessation of PLX5622 treatment peripheral CX3CR1^{+} cells appeared to occupy the majority of the retina area (*D*, *I*, *L*, and *M*), and at 3 mo, the retina is completely repopulated by peripheral CX3CR1^{+} cells (*E*, *J*, *L*, and *M*). The number of repopulated peripheral CX3CR1^{+} cells at 3 mo after the end of PLX5622 treatment approximates that of naive CX3CR1$^{+/EGFP}$ mice with no PLX5622 treatment (*F*, *K*, *L*, and *M*). (*N*) Repopulating peripheral CX3CR1^{+} cells migrated into all three distinct microglia strata (GCL, IPL/INL, and OPL) 3 mo after the injury. (*O*) A cross-section of the retina shows the presence of CX3CR1^{+} cells in the GCL, IPL/INL, and OPL. (*P*) A histogram of CX3CR1$^{+/EGFP}$ expression within the retinal tissue shows intensity peaks of EGFP signal in the GCL, IPL/INL, and OPL. (*Q*) Schematic showing reapplication of PLX5622 in repopulated peripheral microglia. (*R* and *S*) Peripheral monocytes that repopulate the retina remain sensitive to CSF1R inhibition and can be redepleted by reapplication of PLX5622 treatment. (*T*) A representative schematic of a flat-mount retina as used for confocal imaging. The center white circle represents the optic nerve head, red lines represent the retinal vessels, and green dots represent the peripheral monocytes. (*U*) Quantification of peripheral CX3CR1^{+} cells after reapplication of PLX5622 shows complete depletion of repopulated CX3CR1^{+} cells. $n = 5$ mice per group.

tissue-resident macrophages through a monocytic intermediate (29, 30), which could give rise to tissue-resident macrophages postembryonically (29). From our study, it appears that local cues, such as chemokine and cytokine expression in the retina (1), may be pivotal in determining the type of erythromyeloid progenitor (EMP) cells (early or late) recruited into the adult retina, without excluding the possibility that both EMP waves originate from a single population that matures into CSF1R^{+} and CSF1R^{-} cells (29).

Interestingly, CSF1 and IL-4 did not lead to survival of retinal peripherally engrafted CX3CR1^{+} CSF1R^{-} cells (Fig. 4*N*), suggesting that other signals may be involved in the proliferation of these cells in vivo. Moreover, the resistance of CX3CR1^{+} cells to PLX5622 was likely due to reduced CSF1R expression (Fig. 4 *M*

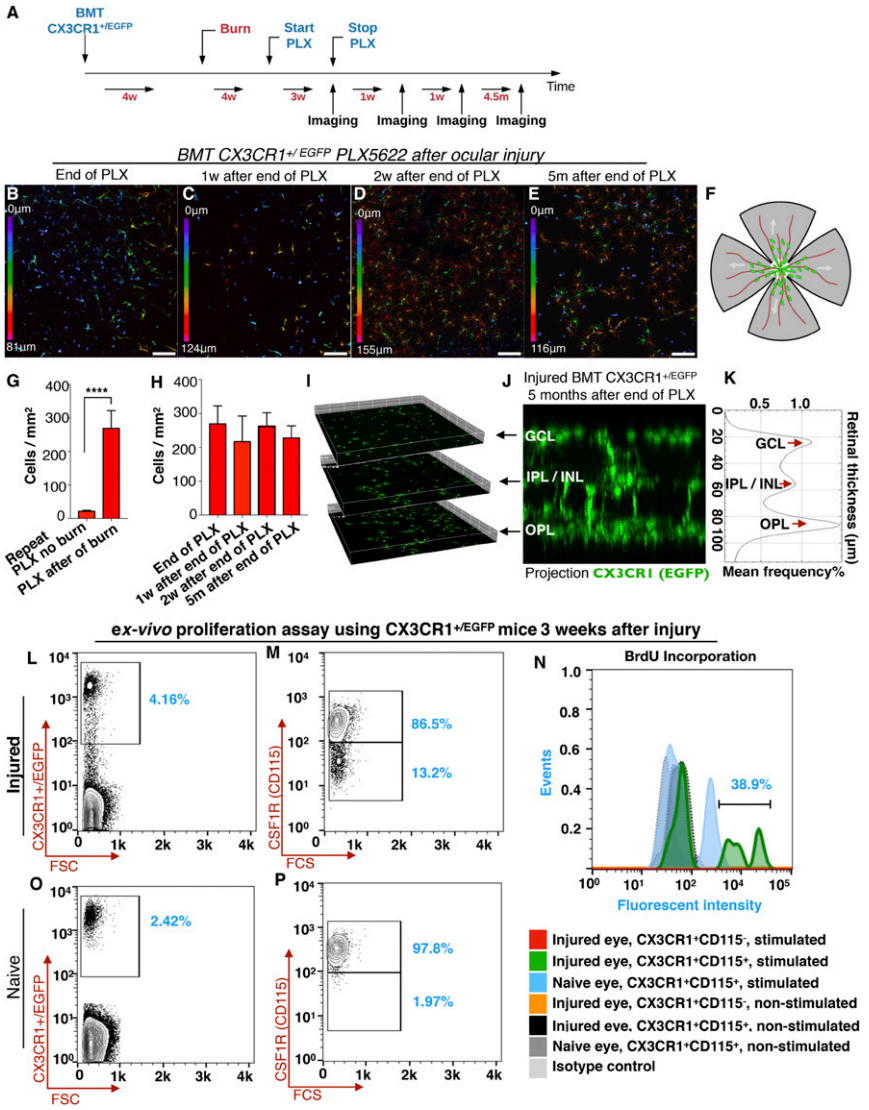

Fig. 4. Ocular injury leads to population of the retina by peripheral CX3CR1$^+$ cells that are resistant to the CSF1R inhibitor. (*A*) Schematic of the experiment: Busulfan-myelodepleted, CX3CR1$^{+/EGFP}$ bone-marrow chimeras received ocular injury and 4 wk later received PLX5622 treatment for 3 wk. (*B* and *G*) Immediately after cessation of PLX5622 treatment, peripherally derived, retina-repopulating CX3CR1$^+$ cells remained present in the retina (*B*) and were resistant to CSF1R inhibition, unlike peripherally derived retina-repopulating CX3CR1$^+$ cells in the absence of ocular injury (*G*). ****$P < 0.0001$; independent *t* test. (*C*–*E* and *H*) One week (*C*), 2 wk (*D*), and 5 mo (*E*) after cessation of PLX5622 treatment peripherally populating CX3CR1$^+$ cells remained present in the retina (*H*) with unchanged cell number. Depth color-coding in *B*–*E*: 0 represents innermost retina. (Scale bars: 100 μm in *B*–*E*.) (*F*) A representative schematic of a flat-mount retina as used for confocal imaging. The center white circle represents the optic nerve head, red lines represent the retinal vessels, and green dots represent the peripheral monocytes. (*I*–*K*) Inhibition-resistant peripheral CX3CR1$^+$ cells that were localized primarily in the GCL/IPL in the early stages after repopulation (see the depth color-code in *B*–*E*) migrated into all three distinct microglia strata 5 mo after the injury with unusually increased cell density in the OPL. (*L*–*P*) Ex vivo functional analysis using flow cytometry of CSF1R$^+$ and CSF1R$^-$ CX3CR1$^+$ retina cells isolated from CX3CR1$^{+/EGFP}$ mice 3 wk after ocular injury or from naive mice. (*L* and *M*) Three weeks after the ocular injury, 86.5% of the CX3CR1$^+$ retinal cells were CSF1R$^+$ (CD115$^+$), and 13.2% were CSF1R$^-$ (CD115$^-$). (*O* and *P*) In naive eyes, 97.8% of retinal CX3CR1$^+$ cells were CSF1R$^+$ (CD115$^+$), and 1.97% were CSF1R^{lo} (CD115^{lo}). (*N*) CSF1R$^-$ and CSF1R$^+$ cells were cultured for 5 d with or without recombinant CSF1 and IL-4 stimulation. BrdU was used in the culture to assess cell proliferation. CSF1R$^-$ cells from both naive and injured eyes were not influenced or rescued by CSF1 and IL-4 stimulation, and cells did not survive the 5-d culture. In contrast, CSF1R$^+$ cells were rescued with CSF1 and IL-4 stimulation and showed increased proliferation and BrdU retention. $n = 3$ mice per group.

and *P* and *SI Appendix*, Fig. S2), but this requires further detailed investigation. In contrast, CX3CR1$^+$ CSF1R$^+$ cells explanted from the retina showed high dependency on CSF1 and IL-4, and stimulation caused proliferation and survival in vitro. Although CSF1 and IL-4 signals are required for microglia proliferation and survival (16, 19, 31), it appears that some monocytes may possess distinct survival strategies. A previous study by Hawley et al. (32) showed that distinct populations of peritoneal macrophages have different dependency on CSF1 levels, while alveolar macrophage replenishment from BM following irradiation is largely independent of CSF1R (33). In addition, a common dendritic cell-2 subset with major overlap in cellular phenotype with other CD11b$^+$ CD11c$^+$ MHC-II$^+$ monocyte-derived antigen-presenting cells (APCs) expresses lower levels of CSF1R mRNA than monocyte-derived APCs (34, 35), and this population is considered CSF1R independent (36). Given the diversity in macrophage function in response to various stimuli (37), we believe that the CSF1 and IL4 independence of peripherally engrafted monocytes of the retina is likely a result of epigenetic reprogramming of progenitor monocytes rather than a distinct ontogeny. However, this independence is

likely to result in functional changes, given that CSF1 is required for the transdifferentiation of monocytes to tissue-resident macrophages, as previously demonstrated in hepatic macrophages (38). Therefore, the absence or low expression of CSF1R and the consequence of CSF1 independence of peripherally engrafted retinal monocytes may negatively affect retinal tissue homeostasis in the long run. More studies in the single-cell level are necessary to test this hypothesis.

Regardless of the mechanism of cell selection or differentiation of EMPs, the presence of peripheral monocytes in the retina constitutes a major homeostatic change (1, 8, 12, 13). Infiltration of bone-marrow–derived myeloid cells was previously described in disease models such as amyotrophic lateral sclerosis (39), Alzheimer disease (40), scrapie (41), bacterial meningitis (42), and other diseases of the CNS (4). Peripheral monocytes have also been shown to contribute to nerve axon degeneration 42 d after spinal cord injury (25). Our recent work demonstrated that MHC-II$^+$ peripheral monocytes infiltrate into the retina promptly after corneal injury, and these cells mediate inflammation and subsequent neuroretinal tissue damage (1). Furthermore, in a more recent study (43), we showed that microglia replacement by peripheral monocytes promotes neurodegeneration after ocular hypertension or traumatic corneal injury. Here we show that peripheral monocytes that infiltrate into the retina remain MHC-II$^+$ months after infiltration and continue to express high levels of IL-1β and TNF-α inflammatory cytokines despite their otherwise quiescent morphology. We also show that peripherally engrafted cells engage more frequently in phagocytosis of neuroretinal tissue, compared with embryonic microglia. Quiescent microglia have low MHC-II expression, while activated microglia and infiltrated macrophages express high MHC-II expression (1, 8, 44–47). Prolonged MHC-II expression by microglia contributes to neuropathology in multiple sclerosis (48) and in Alzheimer (49) and Parkinson's disease (50). Furthermore, a gradual increase in MHC-II expression in the white matter has been shown to cause myelin loss and cognitive decline in aged human and nonhuman primates (51). Our findings agree with previous studies showing that the presence of peripheral monocytes in the CNS and retina is pathologic and likely contributes to neuroinflammation (1, 8, 12, 13). Prolonged residency of activated monocytes in the retina can lead to progressive gradual neuronal damage and irreversible vision loss, which recapitulates the clinical picture of progressive normotensive glaucomatous damage after acute anterior segment injury and appears clinically as a loss of retina ganglion cells. Indeed, acute ocular injury in mice leads to progressive loss of β3-tubulin$^+$ tissue and optic nerve axonal degeneration, as also demonstrated in this study (*SI Appendix*, Fig. S3). Under normal intraocular pressure this can resemble glaucoma seen in patients with chemical injuries (52–54) and could explain the increased susceptibility to glaucoma in patients who have suffered acute ocular injuries (2, 3, 14, 22). In the setting of ocular injury, ramified CX3CR1$^+$ cells from the bone marrow may occupy and engraft into the three distinct microglia strata, thereby coexisting with embryonically derived microglia, but, as we have shown in this study, they have a distinct proinflammatory phenotype. Thus, modifying these immunological processes either by inhibiting the infiltration of peripheral monocytes or retraining them to suppress their inflammatory phenotype may have therapeutic implications for patients suffering from neurodegenerative diseases secondary to inflammation and injury.

A recent study by Gibbings et al. (55) showed that postnatal donor-derived macrophages that populate the alveolar niche acquire a transcriptional profile (>98%) similar to that of embryonic host-derived alveolar macrophages (55), demonstrating that cell ontogeny may not be the only determinant of the transcriptional fate of donor cells that populate the niche (55). Likewise, a study by van de Laar et al. (56) showed that progenitor yolk-sac–derived macrophages, fetal liver monocytes, and bone-marrow–derived monocytes can efficiently colonize the alveolar niche and become transcriptionally and functionally similar to embryonic alveolar macrophages. However, transferred Kupffer cells and colon and peritoneal macrophages do not efficiently colonize the alveolar niche and do not acquire the signature and functions of embryonic alveolar macrophages (56). In both studies, peripheral monocytes that colonized the niche exhibited elevated MHC-II expression but without differences in their inflammatory profile (55, 56). On the other hand, our study shows that peripheral monocytes that populate the retina after injury have high MHC-II expression and elevated expression of IL-1β and TNF-α inflammatory cytokines compared with yolk-sac–derived microglia. We also showed that these peripherally engrafted cells contribute to progressive neurodegeneration and phagocytosis of the neuroretina. Collectively, the studies by Gibbings (55) and van Der Laar (56) and our study suggest that epigenetic reprogramming of repopulating peripheral monocytes may not be directed exclusively by the niche that supplies the cells but also may be modulated by transient cues present during colonization, such as inflammation. In a recent study assessing the ontogeny of tissue-resident macrophages of various organs, only microglia and, to some extent, epidermal Langerhans cells were found to be yolk-sac–derived (57). Therefore, the difference in the inflammatory expression of repopulating alveolar (55, 56) vs. retina macrophages may stem from differences in niche requirements to support resident macrophages as well as from local cues that may be present in the niche during engraftment.

Another important finding of this study is the involvement of microglia in the regulation of peripheral monocyte infiltration into the retina. In the presence of microglia, peripheral CX3CR1$^+$ cells are unable to infiltrate into the retina, and their presence is limited to the area around the optic nerve head (1, 8) (Fig. 1). In contrast, ocular injury or retina microglia depletion causes repopulation from peripheral CX3CR1$^+$ monocytes that are CSF1R$^+$ (Figs. 1 and 3). It is important to mention that microglia depletion is a nonphysiological event that disturbs homeostasis and therefore likely contributes to the deregulation of the neuroglia system. Indeed, microglia depletion with PLX5622 leads to repopulation primarily from peripheral monocytes (~93%) and secondarily from nonperipheral progenitors (7%). In the setting of ocular injury, the contribution from nonperipheral progenitors increases to 20%, which is still relatively low. The inability of nonperipheral microglia progenitors to supply the cells required for prompt repopulation may be due to the nature of microglia, which are long-lived self-renewing cells with a low basal turnover rate (28, 58). In the setting of acute microglia depletion, peripheral monocytes seem to be necessary to support the process of repopulation and overcome the slow turnover rate of microglia progenitors. The ability of CSF1R-independent embryonic precursors to functionally replace yolk-sac–derived microglia during development has been demonstrated (30), suggesting that other tissue macrophages may assume the role of microglia under certain conditions. Our findings are in disagreement with a recent report showing that peripheral monocytes have little contribution to microglia repopulation following PLX5622 treatment (59). Both studies confirm the existence of two distinct CX3CR1$^+$ cell populations (peripheral and central), but their relative contributions differ. Perhaps differences in the fate-mapping techniques used may explain this disparity. Here we used busulfan myelodepletion, which was previously shown not to result in artificial peripheral monocyte infiltration into the retina (1, 4). However, instead of BMT, the contrasting study (59) employed a CX3CR1^{creERT2}-tdTomato model in which most, but not all, peripheral tdTomato$^+$ monocytes are lost 3 mo after tamoxifen induction (60) while microglia retain tdTomato (58, 61). Because not all peripheral tdTomato$^+$ monocytes are lost, it is possible that peripheral monocytes repopulating the retina may arise from a specific peripheral monocyte subpopulation that has not lost tdTomato expression and that lives

significantly longer once engrafted into the tissue. Further studies are needed to resolve this discrepancy.

In conclusion, we have demonstrated that a surface injury to the eye can cause not only peripheral monocyte infiltration into the retina but also permanent engraftment and integration into the neuroretinal tissue, morphologically resembling yolk-sac–derived microglia. However, despite this resemblance, peripherally derived microglia are functionally distinct from yolk-sac–derived ones, remaining activated for the long term, expressing MHC-II, being involved in active phagocytosis of neuronal tissue, and becoming resistant to CSF1R inhibition. These features are not due to their peripheral origin; in the absence of ocular injury, peripherally monocytes that repopulate the retina after PLX5622 treatment remain sensitive to CSF1R inhibition and are MHC-II^{lo}. This observed microglia remodeling contributes to progressive neurodegeneration, which clinically recapitulates the progressive glaucomatous damage to the retina observed in patients with similar ocular injuries. Therefore, modifying this phenotype of peripheral monocytes that contribute to inflammatory microglial remodeling may have clinical therapeutic implications in diseases in which continued neuroinflammatory processes contribute to neurodegeneration.

Materials and Methods

Mouse Model of Alkali Burn. All animal-based procedures were performed in accordance with the Association for Research in Vision and Ophthalmology Statement for the Use of Animals in Ophthalmic and Vision Research. This study was approved by the Animal Care Committee of the Massachusetts Eye and Ear Infirmary. Mice were bred in-house at the Massachusetts Eye and Ear Infirmary Animal Facility and were used at the age of 6–12 wk. CX3CR1^{CreERT2}::ROSA26-tdTomato mice were generated by breeding male B6.129P2(C)-Cx3cr1$^{tm2.1(cre/ERT2)Jung}$/J mice with female B6.Cg-Gt(ROSA)26Sor$^{tm14(CAG-\ tdTomato)Hze}$/J mice. CX3CR1$^{+/EGFP}$/::CCR2$^{+/RFP}$ mice were generated by breeding male B6.129(Cg)-*Ccr2*$^{tm2.1Ifc}$/J mice with female B6.129P-*Cx3cr1*^{tm1Litt}/J mice. The breeding schemes are described in *SI Appendix*, Fig. S4. The following strains were obtained from Jackson Laboratory: C57BL/6J (stock no. 000664), B6.129P-*Cx3cr1*^{tm1Litt}/J (CX3CR1$^{EGFP/EGFP}$) (stock no. 005582) (62), B6.129(Cg)-*Ccr2*$^{tm2.1Ifc}$/J (CCR2$^{RFP/RFP}$) (stock no. 017586) (63), *B6.129P2(C)-CX3CR1*$^{tm2.1(cre/ERT2)Jung}$/J (stock no. 020940) (64), and B6.Cg-Gt(ROSA)26Sor$^{tm14(CAG-\ tdTomato)Hze}$/J (stock no. 007914) (65).

Alkali chemical burns were performed according to our previous study (14). In brief, mice were anesthetized using ketamine (60 mg/kg) and xylazine (6 mg/kg), and deep anesthesia was confirmed by toe pinch. A proparacaine hydrochloride USP 0.5% ophthalmic solution (Bausch and Lomb) was applied to the cornea and after 1 min was carefully dried with a Weck-Cel (Beaver Visitec International, Inc.). A 2-mm-diameter filter paper was soaked in 1 M sodium hydroxide (NaOH) solution for 10 s, dried of excess alkali, and applied onto the mouse cornea for 20 s. After the filter paper was removed, prompt irrigation with sterile saline was applied for 10 s. The mouse was then positioned laterally on a heating pad, and the eye was irrigated for another 15 min at low pressure using sterile saline. Buprenorphine hydrochloride (0.05 mg/kg) (Buprenex Injectable; Reckitt Benckiser Healthcare, Ltd.) was administered s.c. for pain management. A single drop of topical Polytrim antibiotic (polymyxin B/trimethoprim; Bausch & Lomb, Inc.) was administered after the irrigation. Mice were kept on the heating pad until fully awake.

Tissue Preparation for Flat-Mount Imaging. Following the alkali burn, eyes were enucleated at predetermined time points and fixed in 4% paraformaldehyde (PFA) solution (Sigma-Aldrich) for 1 h at 4 °C. The cornea and retina tissue were carefully excised using microsurgical techniques and were washed three times (5 min each washing) in PBS (Sigma-Aldrich) at 4 °C. The tissues were then incubated in 5% BSA (Sigma-Aldrich) and permeabilized using 0.3% Triton-X (Sigma-Aldrich) for 1 h at 4 °C. The specific antibody was added in blocking solution, incubated overnight at 4 °C, and then washed three times (10 min each washing) with 0.1% Triton-X in PBS. The tissues were transferred from the tube to positively charged glass slides using a wide pipette tip with the concave face upward. Four relaxing incisions were made from the center to the periphery to generate four flat tissue quadrants. VECTASHIELD mounting medium (H-1000; Vector Laboratories) was placed over the tissue followed by a coverslip.

Paraphenylenediamine Staining of Optic Nerves. Optic nerve cross sections were processed using a modified paraphenylenediamine (PPD) staining protocol to stain the myelin sheath of all axons and the axoplasma of damaged axons, as previously described (66). Optic nerves were fixed with half-strength Karnovsky's fixative [2% formaldehyde + 2.5% glutaraldehyde in 0.1 M sodium cacodylate buffer, pH 7.4 (Electron Microscopy Sciences)] for a minimum of 24 h at 40 °C. After fixation, samples were rinsed with 0.1 M sodium cacodylate buffer, postfixed with 2% osmium tetroxide in 0.1 M sodium cacodylate buffer, dehydrated with graded ethyl alcohol solutions, and transitioned with propylene oxide and resin infiltrated in tEPON-812 epoxy resin (Tousimis). Optic nerve cross-sections (1 μm) were stained with filtered 2% aqueous PPD (MP Biomedicals, LLC) solution for 1 h at room temperature, rinsed in tap and deionized water solutions, and air-dried. Mounting medium and a glass coverslip were applied over the sections for light microscopic analysis.

Retinal Flat-Mount Imaging. The tissues were prepared for flat mounts and were imaged using a confocal microscope (Leica SP8; Leica Microsystems, Inc.). Images were taken using 10×, 20×, 40×, and 63× objective lenses and z-stacks of 0.7-, 0.6-, 0.4-, and 0.3-μm step sizes, respectively. Image processing was performed with ImageJ version 1.52h software (NIH) to obtain maximum and average projections of the *z* axis, color depth maps, and 3D volumetric images. Amira software v.6 (Thermo Fisher Scientific) was used to perform 3D rendering of confocal images. The number and density of retinal microglia/macrophage cells were quantified using ImageJ software. Retinal flat-mount quantification was performed by averaging the results of one central image (20×) and four peripheral images (20×) of the four retinal quadrants of each retina ($n = 5$). Color-coding analysis of retinal confocal stacks was performed to provide a visual representation of cell density in different retinal strata. A heat map was generated with cold colors (violet–blue) representing the inner retina. The retinal cross-sectional projection was generated from confocal stacks using ImageJ software, and the retinal thickness was calculated by multiplying the number of serial stacks by the step size (in micrometers) of each stack. This information is provided automatically by the LASX v. 1.9.0.13747.1 software of the Leica SP8 confocal microscope (Leica Microsystems, Inc.).

Bone-Marrow Chimera Model. C57BL/6J mice were myelodepleted with three i.p. injections of busulfan (35 mg/kg; Sigma-Aldrich), an alkylating agent that depletes bone-marrow cells, 7, 5, and 3 d before BMT. CX3CR1$^{+/EGFP}$::CCR2$^{+/RFP}$, B6::CX3CR1$^{+/EGFP}$, and CX3CR1^{CreERT2}::ROSA26-tdTomato bone-marrow cells (5×10^6 total bone-marrow cells) were transferred to the myelodepleted C57BL/6J mice through tail vein injection 1 mo before corneal alkali burn. Bactrim (trimethoprim/sulfamethoxazole resuspended in 400 mL drinking water) was given ad libitum for 15 d after busulfan treatment.

Flow Cytometric Analysis of Retinal Cells. Retinas from the harvested eyes were isolated surgically, digested with the Papain Dissociation System (Worthington Biochemical Corporation), and processed with flow cytometry. Retinal microglia/macrophage cells were detected as the EGFP$^+$ or tdTomato population in CX3CR1$^{+/EGFP}$ and CX3CR1^{CreERT2}::ROSA26-tdTomato mice, respectively. Different fluorescent CD45 (clone: 104), CD11b (clone: M1/70), I-A/I-E (MHC-II) (clone: M5/114.15.2), CX3CR1 (clone: SA011F11), Ly6C (clone: HK1.4), and Ly6G (clone: 1A8) antibodies (BioLegend) were used to perform the flow cytometry. Cells were analyzed on a BD LSR II cytometer (BD Biosciences) using FlowJo software (Tree Star).

Evaluation of the Inflammatory Response of Peripherally Engrafted Monocytes After Ocular Injury. Myelodepleted C57BL/6 mice received adoptive transfer of CX3CR1$^{+/EGFP}$ bone-marrow cells and were subjected to corneal injury using 1N NaOH. Sixteen weeks after the injury, the mice were killed, and retinal tissues were surgically removed for enzymatic digestion. CX3CR1$^+$ cells were enriched by FACS, and RNA was isolated from CX3CR1$^+$ cells by using the QIAGEN RNeasy Micro Kit (Qiagen). cDNA was generated using Invitrogen's SuperScript III Reverse Transcriptase (Thermo Fisher Scientific) per the manufacturer's recommendation, and TNF-α (Mm99999068_m1, no. 4331182), IL-1b (Mm00434228_m, no. 4331182), and 18S (Hs99999901_s1, no. 4331182) gene expression was quantified using qPCR and Taqman probes (Thermo Fisher Scientific). qPCR data were analyzed using the ΔΔCt method.

Ex Vivo Proliferation Assay of CSF1R$^-$ Peripherally Engrafted Monocytes. CX3CR1$^{+/EGFP}$ mice were subjected to corneal injury using 1N NaOH. Three weeks later the mice were killed, and retinal tissues were surgically dissected for enzymatic digestion. The single-cell suspension was stained with PE-CD115 (CSF1R) before FACS. CX3CR1$^+$ CD115$^+$ and CX3CR1$^+$ CD115$^-$ cells were sorted separately and used for cell culture with or without stimulation

with 10 ng/mL m-CSF (no. 315-02; PeproTech) and 10 ng/mL IL-4 (no. 214-14; PeproTech) in the presence of BrdU (no. 423401; BioLegend) for 5 d. At the end of coculture (5 d), cells were trypsinized, fixed with 4% PFA, permeabilized with 0.5% Triton-X100 (Sigma-Aldrich), and stained with APC anti-BrdU antibody (no. 339807; Biolegend) for evaluation of BrdU incorporation by flow cytometry.

Microglia Depletion. Microglia depletion was performed using PLX5622, a CSF1R inhibitor. The compound was provided by Plexxikon, Inc. and was formulated in AIN-76A standard chow by Research Diets, Inc. A dose of 1,200 ppm was given to mice for 3 wk.

Statistical Analysis. Results were analyzed with SPSS version 17.0 software (Statistical Package for the Social Sciences, Inc.). The normality of continuous variables was assessed using the Kolmogorov–Smirnov test. All tests were two-tailed, and statistical significance was determined at $P < 0.05$. The independent Student's *t* test was used for comparisons between two groups, and the pairwise *t* test was used to compare changes within the same group. Alpha-level correction was applied, as appropriate, for multiple comparisons.

ACKNOWLEDGMENTS. We thank Pui-Chuen Hui for help in reviewing the manuscript and the members of the Massachusetts Eye and Ear Infirmary animal facility. This work was supported by the Boston Keratoprosthesis Research Fund; Massachusetts Eye and Ear Infirmary; the Eleanor and Miles Shore Fund; the Massachusetts Lions Eye Research Fund; an unrestricted grant to the Department of Ophthalmology, Harvard Medical School from Research to Prevent Blindness (RPB); NIH National Eye Institute Core Grant P30EY003790; the Yeatts Family Foundation Monte J. Wallace Chair; a Macula Society Research Grant; an RPB Physician-Scientist Award; National Eye Institute (NEI) Grant R21EY023079; NEI Grant EY014104 (Massachusetts Eye and Ear Infirmary Core Grant); the Loeffler Family Fund; NEI Grant R01EY025362-01; and an Alcon Research Institute Young Investigator Award.

1. Paschalis EI, et al. (2018) The role of microglia and peripheral monocytes in retinal damage after corneal chemical injury. *Am J Pathol* 188:1580–1596.
2. Cade F, Grosskreutz CL, Tauber A, Dohlman CH (2011) Glaucoma in eyes with severe chemical burn, before and after keratoprosthesis. *Cornea* 30:1322–1327.
3. Crnej A, et al. (2014) Glaucoma progression and role of glaucoma surgery in patients with Boston keratoprosthesis. *Cornea* 33:349–354.
4. Kierdorf K, Katzmarski N, Haas CA, Prinz M (2013) Bone marrow cell recruitment to the brain in the absence of irradiation or parabiosis bias. *PLoS One* 8:e58544.
5. Butovsky O, et al. (2014) Identification of a unique TGF-β-dependent molecular and functional signature in microglia. *Nat Neurosci* 17:131–143.
6. Bennett ML, et al. (2016) New tools for studying microglia in the mouse and human CNS. *Proc Natl Acad Sci USA* 113:E1738–E1746.
7. Streit WJ (2002) Microglia as neuroprotective, immunocompetent cells of the CNS. *Glia* 40:133–139.
8. Kettenmann H, Hanisch UK, Noda M, Verkhratsky A (2011) Physiology of microglia. *Physiol Rev* 91:461–553.
9. Guadagno J, Xu X, Karajgikar M, Brown A, Cregan SP (2013) Microglia-derived TNFα induces apoptosis in neural precursor cells via transcriptional activation of the Bcl-2 family member Puma. *Cell Death Dis* 4:e538.
10. Ajami B, Bennett JL, Krieger C, Tetzlaff W, Rossi FM (2007) Local self-renewal can sustain CNS microglia maintenance and function throughout adult life. *Nat Neurosci* 10:1538–1543.
11. Mildner A, et al. (2007) Microglia in the adult brain arise from Ly-6ChiCCR2+ monocytes only under defined host conditions. *Nat Neurosci* 10:1544–1553.
12. Evans TA, et al. (2014) High-resolution intravital imaging reveals that blood-derived macrophages but not resident microglia facilitate secondary axonal dieback in traumatic spinal cord injury. *Exp Neurol* 254:109–120.
13. Wynn TA, Vannella KM (2016) Macrophages in tissue repair, regeneration, and fibrosis. *Immunity* 44:450–462.
14. Paschalis EI, et al. (2017) Mechanisms of retinal damage after ocular alkali burns. *Am J Pathol* 187:1327–1342.
15. Chen H, et al. (2018) Commensal microflora-induced T cell responses mediate progressive neurodegeneration in glaucoma. *Nat Commun* 9:3209, and erratum (2018) 9: 3914.
16. Elmore MR, et al. (2014) Colony-stimulating factor 1 receptor signaling is necessary for microglia viability, unmasking a microglia progenitor cell in the adult brain. *Neuron* 82:380–397.
17. Dagher NN, et al. (2015) Colony-stimulating factor 1 receptor inhibition prevents microglial plaque association and improves cognition in 3xTg-AD mice. *J Neuroinflammation* 12:139.
18. Gómez-Nicola D, Fransen NL, Suzzi S, Perry VH (2013) Regulation of microglial proliferation during chronic neurodegeneration. *J Neurosci* 33:2481–2493.
19. Jenkins SJ, et al. (2013) IL-4 directly signals tissue-resident macrophages to proliferate beyond homeostatic levels controlled by CSF-1. *J Exp Med* 210:2477–2491.
20. Sauter KA, et al. (2016) Macrophage colony-stimulating factor (CSF1) controls monocyte production and maturation and the steady-state size of the liver in pigs. *Am J Physiol Gastrointest Liver Physiol* 311:G533–G547.
21. Wendeln AC, et al. (2018) Innate immune memory in the brain shapes neurological disease hallmarks. *Nature* 556:332–338.
22. Dohlman CH, et al. (2018) Chemical burns of the eye: The role of retinal injury and new therapeutic possibilities. *Cornea* 37:248–251.
23. Bruttger J, et al. (2015) Genetic cell ablation reveals clusters of local self-renewing microglia in the mammalian central nervous system. *Immunity* 43:92–106.
24. Gosselin D, et al. (2014) Environment drives selection and function of enhancers controlling tissue-specific macrophage identities. *Cell* 159:1327–1340.
25. Greenhalgh AD, David S (2014) Differences in the phagocytic response of microglia and peripheral macrophages after spinal cord injury and its effects on cell death. *J Neurosci* 34:6316–6322.
26. Lavin Y, et al. (2014) Tissue-resident macrophage enhancer landscapes are shaped by the local microenvironment. *Cell* 159:1312–1326.
27. Yamasaki R, et al. (2014) Differential roles of microglia and monocytes in the inflamed central nervous system. *J Exp Med* 211:1533–1549.
28. Shemer A, Erny D, Jung S, Prinz M (2015) Microglia plasticity during health and disease: An immunological perspective. *Trends Immunol* 36:614–624.
29. Ginhoux F, Guilliams M (2016) Tissue-resident macrophage ontogeny and homeostasis. *Immunity* 44:439–449.
30. Hoeffel G, et al. (2015) C-Myb(+) erythro-myeloid progenitor-derived fetal monocytes give rise to adult tissue-resident macrophages. *Immunity* 42:665–678.
31. Sehgal A, et al. (2018) The role of CSF1R-dependent macrophages in control of the intestinal stem-cell niche. *Nat Commun* 9:1272.
32. Hawley CA, et al. (2018) *Csf1r*-mApple transgene expression and ligand binding in vivo reveal dynamics of CSF1R expression within the mononuclear phagocyte system. *J Immunol* 200:2209–2223.
33. Hashimoto D, et al. (2013) Tissue-resident macrophages self-maintain locally throughout adult life with minimal contribution from circulating monocytes. *Immunity* 38:792–804.
34. Cerovic V, et al. (2013) Intestinal CD103(-) dendritic cells migrate in lymph and prime effector T cells. *Mucosal Immunol* 6:104–113.
35. Schlitzer A, et al. (2013) IRF4 transcription factor-dependent CD11b+ dendritic cells in human and mouse control mucosal IL-17 cytokine responses. *Immunity* 38:970–983.
36. Guilliams M, et al. (2014) Dendritic cells, monocytes and macrophages: A unified nomenclature based on ontogeny. *Nat Rev Immunol* 14:571–578.
37. Hume DA (2015) The many alternative faces of macrophage activation. *Front Immunol* 6:370.
38. Stutchfield BM, et al. (2015) CSF1 restores innate immunity after liver injury in mice and serum levels indicate outcomes of patients with acute liver failure. *Gastroenterology* 149:1896–1909.e1814.
39. Solomon JN, et al. (2006) Origin and distribution of bone marrow-derived cells in the central nervous system in a mouse model of amyotrophic lateral sclerosis. *Glia* 53: 744–753.
40. Malm TM, et al. (2005) Bone-marrow-derived cells contribute to the recruitment of microglial cells in response to beta-amyloid deposition in APP/PS1 double transgenic Alzheimer mice. *Neurobiol Dis* 18:134–142.
41. Priller J, et al. (2006) Early and rapid engraftment of bone marrow-derived microglia in scrapie. *J Neurosci* 26:11753–11762.
42. Djukic M, et al. (2006) Circulating monocytes engraft in the brain, differentiate into microglia and contribute to the pathology following meningitis in mice. *Brain* 129: 2394–2403.
43. Paschalis EI, et al. (2018) Microglia regulate neuroglia remodeling in various ocular and retinal injuries. *J Immunol,* in press.
44. Berman NE, et al. (1999) Microglial activation and neurological symptoms in the SIV model of NeuroAIDS: Association of MHC-II and MMP-9 expression with behavioral deficits and evoked potential changes. *Neurobiol Dis* 6:486–498.
45. Mittal R, et al. (2010) IL-10 administration reduces PGE-2 levels and promotes CR3-mediated clearance of Escherichia coli K1 by phagocytes in meningitis. *J Exp Med* 207: 1307–1319.
46. Mizutani M, et al. (2012) The fractalkine receptor but not CCR2 is present on microglia from embryonic development throughout adulthood. *J Immunol* 188:29–36.
47. Hambardzumyan D, Gutmann DH, Kettenmann H (2016) The role of microglia and macrophages in glioma maintenance and progression. *Nat Neurosci* 19:20–27.
48. Hayes GM, Woodroofe MN, Cuzner ML (1987) Microglia are the major cell type expressing MHC class II in human white matter. *J Neurol Sci* 80:25–37.
49. Perlmutter LS, Scott SA, Barrón E, Chui HC (1992) MHC class II-positive microglia in human brain: Association with Alzheimer lesions. *J Neurosci Res* 33:549–558.
50. Imamura K, et al. (2003) Distribution of major histocompatibility complex class II-positive microglia and cytokine profile of Parkinson's disease brains. *Acta Neuropathol* 106:518–526.
51. Sheffield LG, Berman NE (1998) Microglial expression of MHC class II increases in normal aging of nonhuman primates. *Neurobiol Aging* 19:47–55.
52. Wakefield D, Lloyd A (1992) The role of cytokines in the pathogenesis of inflammatory eye disease. *Cytokine* 4:1–5.
53. Neri P, Azuara-Blanco A, Forrester JV (2004) Incidence of glaucoma in patients with uveitis. *J Glaucoma* 13:461–465.
54. Inman DM, Horner PJ (2007) Reactive nonproliferative gliosis predominates in a chronic mouse model of glaucoma. *Glia* 55:942–953.
55. Gibbings SL, et al. (2015) Transcriptome analysis highlights the conserved difference between embryonic and postnatal-derived alveolar macrophages. *Blood* 126: 1357–1366.

56. van de Laar L, et al. (2016) Yolk sac macrophages, fetal liver, and adult monocytes can colonize an empty niche and develop into functional tissue-resident macrophages. *Immunity* 44:755–768.
57. Sheng J, Ruedl C, Karjalainen K (2015) Most tissue-resident macrophages except microglia are derived from fetal hematopoietic stem cells. *Immunity* 43:382–393.
58. Lawson LJ, Perry VH, Gordon S (1992) Turnover of resident microglia in the normal adult mouse brain. *Neuroscience* 48:405–415.
59. Zhang Y, et al. (2018) Repopulating retinal microglia restore endogenous organization and function under CX3CL1-CX3CR1 regulation. *Sci Adv* 4:eaap8492.
60. van Furth R, Cohn ZA (1968) The origin and kinetics of mononuclear phagocytes. *J Exp Med* 128:415–435.
61. Parkhurst CN, et al. (2013) Microglia promote learning-dependent synapse formation through brain-derived neurotrophic factor. *Cell* 155:1596–1609.
62. Jung S, et al. (2000) Analysis of fractalkine receptor CX(3)CR1 function by targeted deletion and green fluorescent protein reporter gene insertion. *Mol Cell Biol* 20: 4106–4114.
63. Saederup N, et al. (2010) Selective chemokine receptor usage by central nervous system myeloid cells in CCR2-red fluorescent protein knock-in mice. *PLoS One* 5: e13693.
64. Yona S, et al. (2013) Fate mapping reveals origins and dynamics of monocytes and tissue macrophages under homeostasis. *Immunity* 38:79–91.
65. Madisen L, et al. (2010) A robust and high-throughput Cre reporting and characterization system for the whole mouse brain. *Nat Neurosci* 13:133–140.
66. Zhou C, et al. (2017) Sustained subconjunctival delivery of infliximab protects the cornea and retina following alkali burn to the eye. *Invest Ophthalmol Visual Sci* 58: 96–105.